Easy Direct Functionalization of 2D MoS2 Applied in Covalent Hybrids with PANI as Dual Blend Supercapacitive Materials

ADVANCED MATERIALS INTERFACES
Open Access
www.advmatinterfaces.de

Easy Direct Functionalization of 2D MoS_2 Applied in Covalent Hybrids with PANI as Dual Blend Supercapacitive Materials

*Matteo Crisci, Felix Boll, Sara Domenici, Jaime Gallego, Bernd Smarsly, Mengjiao Wang, Francesco Lamberti, Andrea Rubino, and Teresa Gatti**

The pressing demand for more sustainable energy provision and the ongoing transition toward renewable resources underline the critical need for effective energy storage solutions. To address this challenge, scientists persistently explore new compounds and hybrids and, in such a dynamic research field, 2D materials, particularly transition metal di-chalcogenides (TMDCs), show great potential for electrochemical energy storage uses. Simultaneously, also conductive polymers (CPs) are interesting and versatile supercapacitor materials, especially polyaniline (PANI), which is extensively studied for this purpose. In this work, a powerful method to combine TMDCs and PANI into covalently grafted hybrids starting from aniline functionalized few-layers 1T-MoS_2, attained by a facile direct arylation with iodoaniline, is presented. The hybrids provide circa 70 F g^{-1} specific capacitance in a pseudo device setup, coupled with a robust capacitance retention of well over 80% for up to 5000 cycles. These findings demonstrate the potential of similar covalent composites to work as active components for novel, innovative energy storage technologies. At the same time, the successful synthesis marks the efficacy of direct covalent grafting of conductive polymer on the surface of 2D TMDCs for stable functional materials.

1. Introduction

The global shift toward sustainable energy systems is driving an increasing demand for high-performance energy storage solutions. Among the various technologies available, supercapacitors have gained significant attention due to their high power density, rapid charge-discharge cycles, and long cycle life.[1,2] However, the development of materials capable of providing both high energy density and cycle stability remains a key challenge. This has led researchers to explore novel material combinations, particularly the blending of 2D materials with conductive polymers (CPs), to enhance the electrochemical performance of supercapacitors.[3–9]

CPs are often pseudo-capacitive, possess good electrical conductivity and intrinsic capacitance, and are easy to produce. Polyaniline (PANI), a widely studied conducting polymer, has been considered a promising candidate for supercapacitor electrodes due to its pseudocapacitive properties, ease of synthesis, and low cost.[10–13] However, PANI suffers from significant degradation over multiple charge-discharge cycles,[12,14] primarily due to structural changes during the redox process, which leads to a rapid decline in capacitance. This limits its practical application in energy storage devices, necessitating strategies to improve its cycle life and stability.

M. Crisci, F. Boll, J. Gallego, B. Smarsly
Institute of Physical Chemistry
Justus Liebig University
Heinrich Buff Ring 17, 35392 Giessen, Germany

M. Crisci, F. Boll, S. Domenici, J. Gallego, B. Smarsly, T. Gatti
Center for Materials Research
Justus Liebig University
Heinrich Buff Ring 16–17, 35392 Giessen, Germany
E-mail: teresa.gatti@polito.it

The ORCID identification number(s) for the author(s) of this article can be found under https://doi.org/10.1002/admi.202400621

DOI: 10.1002/admi.202400621

S. Domenici, M. Wang, A. Rubino, T. Gatti
Department of Applied Science and Technology
Politecnico di Torino
C.so Duca degli Abruzzi 24, 10129, Torino 10129, Italy

F. Lamberti
Department of Chemical Sciences
University of Padova
Via Marzolo 1, Padova 35131, Italy

F. Lamberti
Department of Industrial Engineering
University of Padova
Via Gradenigo 6a, Padova 35131, Italy

A. Rubino
Functional Nanosystems
Istituto Italiano di Tecnologia
Via Morego 30, Genova 16163, Italy

On the other hand, 2D-MoS_2, a transition metal dichalcogenide (TMDC), has been extensively studied and emerged as an energy storage material, due to its van der Waals and layered structure, allowing for easy ions' intercalation and the high surface area achievable.[15–18] However, MoS_2, particularly in its semiconducting 2H phase, exhibits low electrical conductivity, which limits its ability to deliver high power density, which can be partially improved by using the relative 1T phase, which however is metastable. Additionally, the aggregation of MoS_2 nanosheets during cycling can further reduce its performance over time, therefore spacers can additionally help to reduce this effect. To address these issues, combining the strengths of both materials in a hybrid system has emerged as a promising approach. By blending MoS_2 nanosheets with PANI, it is possible to harness the high surface area and ion intercalation capability of MoS_2 alongside the pseudocapacitive behavior of PANI. Such hybrids can improve the overall electrochemical performance, particularly in terms of capacitance retention and cycle stability,[19–21] by mitigating the weaknesses of each component material. In this work, we present a novel approach to the covalent functionalization of MoS_2 nanosheets with PANI, aiming to create a hybrid material that exhibits enhanced supercapacitive performance. The direct covalent grafting of PANI onto the surface of exfoliated MoS_2 ensures a robust interaction between the two materials, improving charge transfer and structural integrity during cycling. This hybrid structure not only enhances the conductivity of MoS_2 by maintaining the material in its highly conductive 1T phase, but also stabilizes the PANI polymer, thereby improving its cycle life.

Based on this background knowledge, we report a new synthetic protocol for preparing nanohybrids by grafting PANI onto a functionalized 2D MoS_2 NSs (MoS_2@PANI) demonstrating specific capacitances of up to 70 F g^{-1} in a pseudo-device system, exhibiting capacitance retention of over 80% after 5000 cycles, and underscoring the potential of MoS_2-PANI hybrids as next-generation super capacitive materials. This work highlights the efficacy of combining functionalization[22] to obtain specific moieties on the 2D materials and its grafting orientation of conductive polymers, resulting in a robust integration of the two materials,[23] and addressing the long-standing challenges of energy storage, paving the way for the development of more efficient and durable supercapacitors.[12]

2. Results and Discussion

The layered material was obtained by adapting a literature chemical exfoliation procedure, where n-butyllithium was used as an electron donor reactant to foster the phase transition from the 2H-phase, typically existing in the bulk powder, to the 1T-phase, as described in the Experimental Section. The exfoliated MoS_2, obtained from the resulting aqueous-base ink via freeze drying, has been characterized by powder X-ray diffraction (P-XRD) and Raman analysis (see Figure S1, Supporting Information). From Raman spectra, it is possible to observe signatures of both the 1T and 2H phases of MoS_2, while the P-XRD showed the typical reflex of 1T MoS_2 at 8° and the presence of surface oxide, due probably to the oxidation caused by the exfoliation process (see S.I. for further discussion).

Considering the Raman results, X-ray photoelectron spectroscopy (XPS) measurements were also performed to evaluate the quality of the synthesized material and its composition. As displayed in Figure 2a, the Mo 3d region in the XPS spectra shows different signals, which were fitted using three different components for Mo and one for S respectively, since the S 2s (225.8 eV) is present in this region as well. Therein, the XPS peaks at 228.1 and 231.3 eV corresponded to Mo(1T) $3d_{5/2}$ and Mo(1T) $3d_{3/2.}$ While the peaks shifted toward higher binding energy at 229.1 and 232.2 eV are from Mo(2H) $3d_{5/2}$ and Mo(2H) $3d_{3/2}$.[24–26] This shift is due to the higher electron density inside 2H-MoS_2 compared to 1T-MoS_2. Being the different peaks circa 1 eV apart, it is possible to distinguish between the two MoS_2 phases.[27] Based on this result, the ratio between the two phases was calculated from the performed fittings and it suggests an estimated distribution of 70% 1T-MoS_2 and 30% 2H-MoS_2. The high percentage of 1T-phase significantly changes the material properties, allowing for its dissolution in water and easy functionalization in such media, despite the presence of some 2H phase in the final product. Besides, two peaks found at 232.7 and 235.6 eV were attributed respectively to MoO_x $3d_{5/2}$ and MoO_x $3d_{3/2,}$ indicating the existence of MoO_x formed during the synthesis.[24,25,28] The analysis of the S 2p spectral range can provide information correlated to that of the Mo 3d (Figure 2b). The main peak of S 2p is fitted at 160.9, 162, 162.1, and 163.2 eV, which are attributed to S(1T) $2p_{3/2,}$ S(1T) $2p_{1/2,}$ S(2H) $2p_{3/2}$ and S(2H) $2p_{1/2,}$ respectively. Additionally, the peaks at 169.1 and 170.3 eV were attributed to superficial SO_4^{2-}, which is a common impurity in S-based compounds due to air exposure.

With this information acquired, the as-produced 1T-MoS_2 ink was then used for the direct arylation step (**Figure 1**), following a previously reported procedure.[29] Therein, *p*-iodoaniline was used in large excess as a functionalizing agent and the grafting onto 1T-MoS_2 electron rich sulfur atoms was facilitated due to the weak C—I bond in the reagent. However, electron donating moieties in di-substituted iodo-aryls, such as —NH_2 groups, proved to lead to a lower surface grafting compared to electron withdrawing moieties.[29] This effect can be explained using the Hammett parameters theory for di-substituted aryls, where functional groups with a negative Hammett value (electron donating) increase the electron density on the aryl, stabilizing the forming carbo-cation after the —I leaving group and therefore rendering it less reactive.[30–32] To compensate this effect, which opposes the functionalization process, working conditions for this reaction were tuned, testing different reaction times (1, 3, and 7 days, respectively) and increasing the temperature to 40 °C from the previously reported room temperature, to fasten the kinetics of the reaction. After the end of the reaction, the material was collected and purified according to the procedure described in the Experimental Section. Evidence of covalent functionalization was confirmed through XPS spectra of MoS_2 with the functionalization reaction of 1 day (see **Figure** 2c,d). In the Mo3d range, the functionalization's impact on the two materials' phases is evident (Figure 2c). After the fitting, a significant increase in 2H-phase compared to 1T is detected, with proportions reaching 65% and 35%, respectively. Besides, the main peaks associated with MoS_2 remain present, but the peaks corresponding to 1T-MoS_2 appear wider than those of 2H-MoS_2, consistent with the Mo 3d spectrum results (Figure 2c). The S 2p binding energy region provides further valuable information on the functionalization (Figure 2d). In fact, following the reaction, additional peaks can

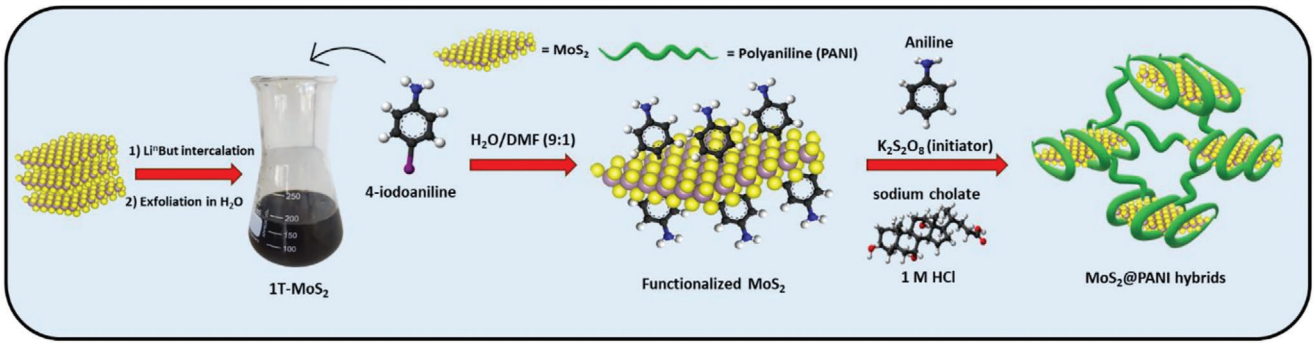

Figure 1. Sketch of the whole synthetic process toward covalent 2D MoS_2/PANI nanohybrids, including chemical exfoliation, 4-iodoaniline functionalization, and PANI covalent grafting.

be observed at 167 and 168.2 eV. These peaks are shifted to higher binding energies compared to the typical assignment of C—S bonds, which are usually reported ≈164 eV. This shift is likely due to changes in electron density around the element, indicating covalent functionalization of MoS_2 with aniline moieties. N 1s XPS profile shown in Figure S2 (Supporting Information) further corroborates the aniline decoration of the MoS_2 surface, since two sharp peaks at 394.6 and 398.9 eV can be deconvoluted and attributed, respectively, to Mo 3p and aniline oligomers (or to polyaniline) according to the NIST XPS database.[33] Therefore, after functionalization, a shift in phase majority occurs: while the 1T-phase is predominant before functionalization, the 2H-phase becomes the dominant component afterward. This transition can be attributed to several factors, primarily the natural conversion of the 1T-phase to 2H over time and the material's instability in an air atmosphere, which causes both phase transition and partial oxidation. Functionalization, however, stabilizes the material, locking the 1T-phase and preventing further changes.

Another evidence of the presence of organic C—S bonds in the materials is provided by the infrared (IR) spectroscopy analysis represented in **Figure** 3a. In the fingerprint region between 500 and 1000 cm^{-1} a peak at 620 cm^{-1} (Figure 3b) appears after the reaction, corresponding to the C—S stretching,[34] which confirms the covalent grafting of aniline moieties onto the MoS_2 surface. However, this peak does not significantly increase with reaction time. The absence of a noticeable increase, which would indicate

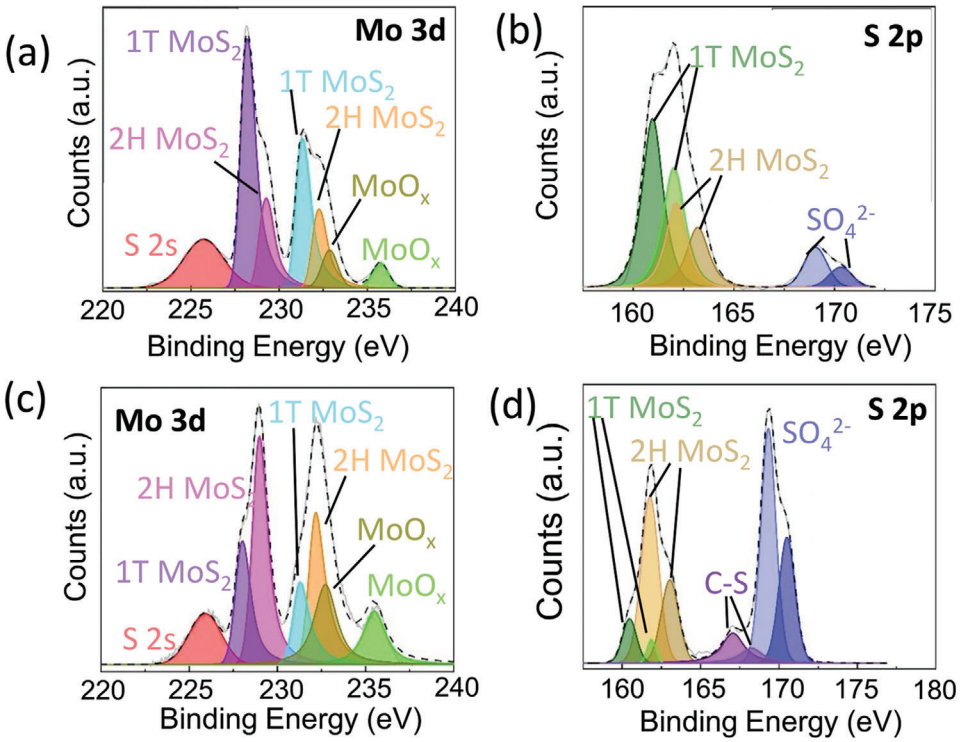

Figure 2. a–d) XPS spectra of 1T-MoS_2 prepared by chemical exfoliation and functionalized for 1 day with 4-iodoaniline. Fitted Mo 3d region before (a) and after (c) functionalization (including the underlying S 2s peak). Fitted S 2p region before (b) and after (d) functionalization.

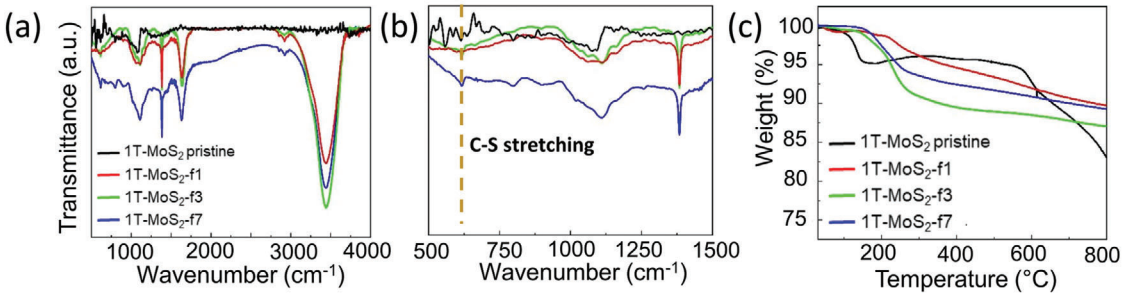

Figure 3. a) IR adsorption spectra of pristine and functionalized MoS_2. (b) is a magnification of (a) in the range of 500–1500 cm^{-1}. c) TGA of pristine and functionalized MoS_2.

a higher presence of the bond, can be attributed to surface saturation, leading to the formation of oligomeric branches rather than additional C—S bonds (see later in the text for more details on this). Several other peaks were observed at 3430, 1632, 1394, and 1108 cm^{-1}, attributed to N—H stretching, N—H bending, C—C stretching, and C—N stretching modes, respectively. These findings additionally point toward the presence of aniline moieties on the surface of the material.

Finally, thermogravimetric analysis (TGA) was carried out on the functionalized MoS_2 to investigate the presence of organic functional moieties on the surface of the material (Figure 2f). The pristine 1T-MoS_2 sample exhibits an initial downward slope ≈120 °C, attributed to the release of interstitial water, followed by a slight increase in the material's weight percentage. This increase may be due to a phenomenon known as tumescence, where heating causes the material to behave like pitch, forming bubbles that can lead to a misinterpretation of the weight before the bubbles are released.[35] This is further confirmed by mass spectrometry data associated with the TGA measurements, where only a sharp peak at 18 m/z peak was observed around the same temperature, which corresponds to the molecular mass of water (see Figure S3, Supporting Information). On the other hand, the functionalized material shows a sharp decrease in mass between 180 and 300 °C. This effect, spanning for more than 100 °C, is the index of gradual and slow degradation of organic species. While pure aniline typically evaporates at ≈180 °C, in this case, the effect can be attributed to a more complex decomposition process rather than the mere detachment of individual aniline moieties from the nanosheets (NSs).[36,37] In fact, this degradation is likely to be attributed to oligomers of aniline. Specifically, whenever the surface of the 2D material has been already functionalized, further addition of monomers can be done on top of the already existing grafted aniline moieties, starting to create oligomers, which are usually called nano-branches, and these compounds decompose in a similar way to polyaniline, as observed in the thermograms in Figure 2f.[36,37] Once the surface functionalization reaches a certain extent, the excess of iodoaniline will preferentially react with already grafted aniline moieties and form PANI-like oligomers on the surface. However, this phenomenon can often lead to a broad and uncontrollable size dispersion of the oligomers on the surface. For this reason, in Figure 2f the 3 days functionalization (MoS_2-*f3*) shows a higher mass loss compared to the 7 days one (MoS_2-*f7*), since the former most probably features a higher degree of oligomers on the surface. Overall, already 1-day of reaction (MoS_2-*f1*) was enough to reach a functionalization degree of 3.6% (in mass fraction, see Table S1, Supporting Information). When the reaction time was increased, the functionalization degree was estimated to reach up to 9.5% per S atom, but this high value can also be attributed to the formation of branches, as previously mentioned.

Transmission electron microscopy (TEM) imaging was employed to characterize the NSs morphology and composition after aniline functionalization. TEM image in **Figure** 4a shows that the MoS_2-f1 NSs feature a size of around half micron. From high-resolution TEM (HRTEM, Figure 4b,c), it is possible to observe a few layered materials and different regions where both the 2H and the 1T-phase of the material were detected (Figure S4, Supporting Information), confirming the results from the XPS fittings (Figure 2a–d) on the presence of both phases in the material, which can even co-exist in a single flake. In addition, scanning TEM (STEM) coupled to energy dispersive x-ray analysis (STEM-EDX) characterization (Figure 4d–f) confirms the presence of both nitrogen and sulfur on the functionalized NSs, with a highly homogeneous distribution of both elements, hinting at an ordered surface decoration of the layered nanomaterial with aniline or its oligomers.

Starting from the aniline-decorated MoS_2 flakes obtained after 1 day of functionalization (MoS_2-f1), 2D MoS_2/PANI hybrids (MoS_2-f1@PANI) were prepared, following the procedure described in the Experimental Section and sketched in Figure 1. In particular, hybrids with a 1:20 molar ratio between the inorganic (functionalized-MoS_2) and organic (PANI) components were synthesized using both the pristine 1T phase and the functionalized one. Briefly, the conducting polymer was prepared in situ, by adding aniline and the oxidizing agent, ammonium peroxidisulfate (APS), as reactants to the dispersed MoS_2-f1 NSs, and the final hybrid was collected as a powder after purification, they were called respectively MoS2(1T)@PANI 1:20 and MoS2-f1@PANI 1:20. The as-synthesized materials were characterized with Raman spectroscopy, P-XRD analysis, scanning electron microscopy (SEM) and EDX and details are discussed in Figure S5 (Supporting Information). In summary, after the polymerization of PANI around the 2D material, the only peaks in the Raman analysis and reflexes in the P-XRD visible are the ones related to the polymer, while SEM pictures show a rod-like morphology, typical of the PANI structure (Figure S6, Supporting Information). On the other hand, EDX reveals the presence of both Mo and S in the material together with C and Cl, confirming the presence of all the expected atomic components in the hybrids. Nitrogen is not seen due to overlap with the EDX signal of carbon; however,

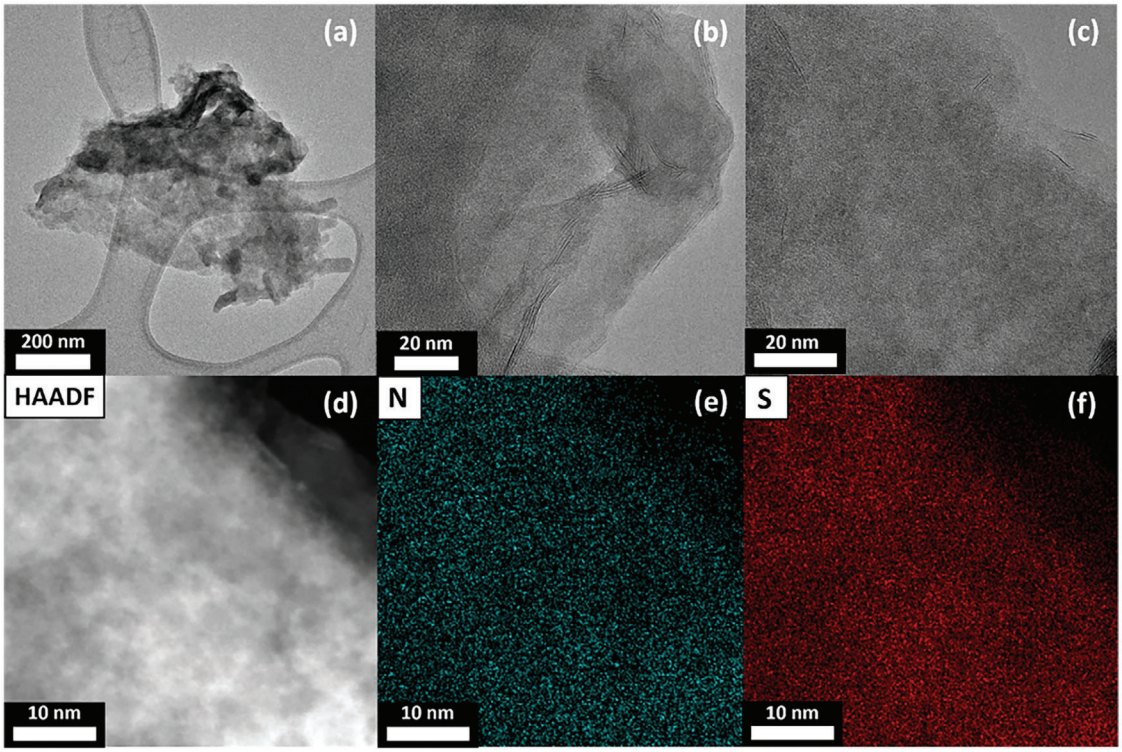

Figure 4. a) TEM and b,c) HR-TEM image of the MoS_2-f1 (i.e., after 1 day functionalization), associated to the corresponding d–f) STEM-EDX image, nitrogen, and sulfur elemental maps.

chlorine is an indirect indicator of the nitrogen presence, since chlorine is the anionic dopant in the PANI emeraldine structure, counterbalancing the positive charges of the —NH—$^+$ moieties.

After characterizing the structural and morphological properties of the MoS_2-f1@PANI hybrid, which was easily produced by the 3-step exfoliation-functionalization-polymerization procedure previously described, its electrochemical behavior was tested in order to investigate the potential for use in supercapacitor-like devices. For comparison, a reference hybrid, termed MoS_2(1T)@PANI, was prepared by in-situ polymerization of aniline in the presence of pristine 1T-MoS_2. Initial analyses were carried out in a 3-electrodes system to study the properties of the hybrid materials and compare them to the pristine components, using H_2SO_4 0.5 M as the electrolyte (see more details in the Experimental Section). Cyclic voltammetry (CV) analysis was first performed to select the potential range suitable for subsequent galvanostatic charge-discharge (GCD) measurements. From **Figure** 5a, it is possible to notice that in almost all samples the PANI redox peaks appear between 0.25 and 0.5 V (vs RHE), therefore GCD measurements performed in this potential window will exploit the pseudo-capacitive storage mechanism related to this redox couple. However, in the hybrid containing the pristine 1T-MoS_2, there is an evident shift and broadening of the PANI oxidative peak toward higher potentials, from 0.4 to 0.7 V. This shift could be explained by an anti-synergistic effect between the inorganic and organic components in the nanohybrid. Previous studies have extensively reported the effect of dopants and additives on the redox behavior of PANI, with inorganic acid being the most reported as the dopant that can change the properties of the conducting polymer. However, there are some examples of inorganic materials[38–40] used in combination with PANI that significantly change the polymer redox properties. Similarly, 1T-MoS_2 may act as an additive for PANI, with its negative surface charge influencing the redox properties of the polymer chains. In contrast, no similar effect is observed when the functionalized material is used (MoS_2-f1@PANI), which behaves instead like pure PANI, thanks to the direct connection between the polymeric part and the inorganic part. This result hints at a different type of interaction between the conducting polymer and the inorganic nanomaterial, compared to the case of the nongrafted hybrid.

With clear information on the redox behavior of the examined systems and by comparing it with previous literature reports, the potential window between 0 and 0.8 V versus RHE was set to explore the capacitive properties of the nanohybrids.[41] GCD curves were subsequently obtained within this potential range, primarily exhibiting nearly ideal shapes, as depicted in Figure 5b and Figure S7 (Supporting Information). These curves typically formed a triangular pattern, with distinct charge and discharge phases. However, the GCD curves in Figure 4b do not display the happening of a faradic process (the PANI redox reaction), as observed in the CV curves. This discrepancy may be due to the value of the current density used for the GCD measurements. The CV was performed at a low scan rate, where a partially reversible redox couple was noticeable. The higher current density applied during the GCD measurements may have however reduced the extent to which the redox surface reactions have the time to take place. From the cycle performance, we can

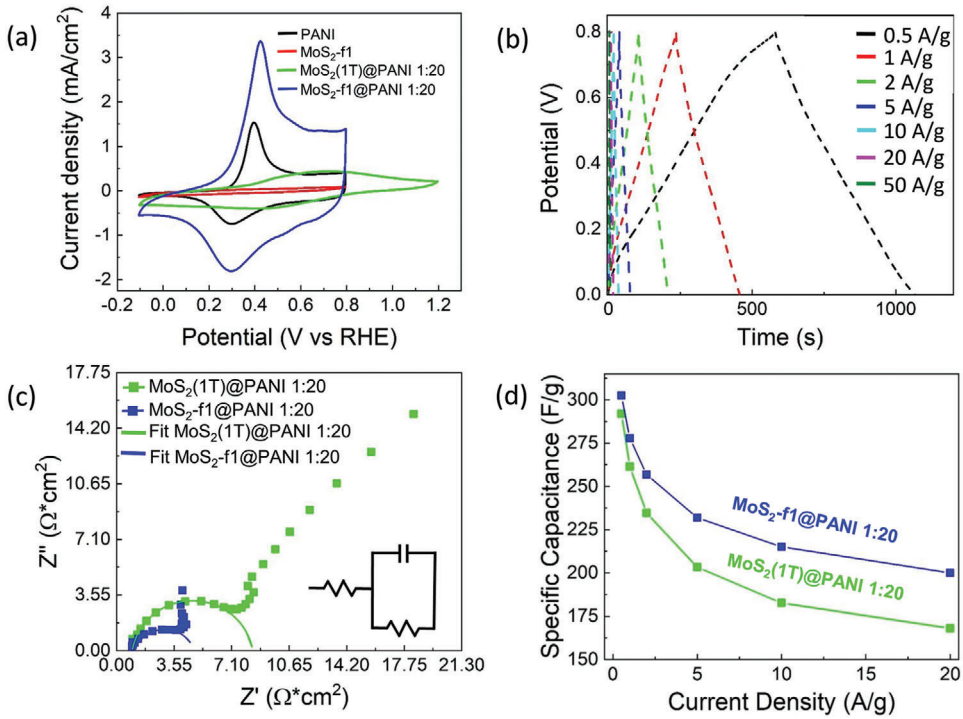

Figure 5. Three-electrodes electrochemical characterization of the covalently grafted and non-grafted 2D MoS_2/PANI hybrids. a) CVs of hybrids and individual components. b) GCD curves for the grafted MoS_2-f1@PANI hybrid at different current densities (see Figure S7, Supporting Information, for the corresponding curves of the non-grafted sample). c) PEIS analysis and d) specific capacitance calculated for the two hybrid materials.

observe a negligible iR drop, which is usually related to the internal resistance of the system. As counter-evidence, potentiostatic electrochemical impedance spectroscopy (PEIS) analysis was performed, and from the relative Nyquist plots a clear difference between the two hybrids emerges (Figure 5c). For both MoS_2-f1@PANI and MoS_2(1T)@PANI samples, the analysis reveals a semicircle at high frequencies, followed by a straight line at lower frequencies, hinting at a similar process happening at the applied potential.[42,43] The functionalized material (MoS_2-f1@PANI) shows a smaller semicircle, compared to the MoS_2(1T)@PANI, corresponding to a lower charge transfer resistance (R_{ct}) and the exact values can be estimated by fitting the corresponding circle with a suitable model (Figure 5c). Moreover, the conductivity can also be extrapolated from these values, and, assuming a similar thickness for both electrodes, the conductivity values support a better charge mobility in the functionalized material. The values presented in Table S2 (Supporting Information) indicate a higher internal resistance for the MoS_2(1T)@PANI hybrid compared to the MoS_2-f1@PANI sample, due to several key factors. One is the stabilization of the metallic 1T-MoS_2 phase in the MoS_2-f1@PANI hybrid, as the 1T-phase is known for its high conductivity, especially when compared to the 2H-phase.[15,17] As mentioned before, functionalization locks the 1T-phase,[44,45] preventing transition to the less conductive 2H-phase, which can occur due to air exposure or continuous cycling. Additionally, the direct covalent grafting of PANI onto the functionalized MoS_2 NSs in the MoS_2-f1@PANI hybrid significantly enhances charge transfer across the interface by strengthening electronic coupling between the PANI and MoS_2 layers, facilitating more efficient electron transport pathways. In contrast, the pristine MoS_2(1T)@PANI sample exhibits weaker interactions between the polymer and MoS_2 nanosheets, resulting in higher R_{ct}. Furthermore, differences in polymerization play a role; in the MoS_2-f@PANI hybrid, covalent bonding ensures uniform polymerization and better integration of PANI with MoS_2, leading to lower charge transfer resistance. Conversely, the less organized structure in the MoS_2(1T)@PANI system increases the impedance. Thus, the differences in conductivity, functionalization, and covalent bonding account for the variations in charge transfer resistance between the two systems. We also conducted PEIS under additional potentials for MoS_2(1T)@PANI and MoS_2-f1@PANI (Figure S8, Supporting Information). The only notable change was the absence of the semicircle in the impedance plots, indicating no surface reactions outside the potentials used in the EIS shown in Figure 5c, where the PANI redox potential peaks are observed.

The GCD results displayed in Figure 5b and Figure S7 (Supporting Information) were used to calculate the values plotted in Figure 5d, using Equation (1) reported in Experimental Section. The hybrids showed a similar specific capacitance (C_s) at low current density (0.5 A g^{-1}) of 302.5 F g^{-1} for the functionalized material-based hybrid and 291 F g^{-1} for the unfunctionalized reference, with only a 3.5% difference between the two species. However, at increasing applied current, the difference becomes more pronounced, reaching a 16% difference in C_s at 20 A g^{-1}, with 200 F g^{-1} for MoS_2-f1@PANI and 168 F g^{-1} for MoS_2(1T)@PANI, pointing at a significant improvement in performance promoted by the surface functionalization.

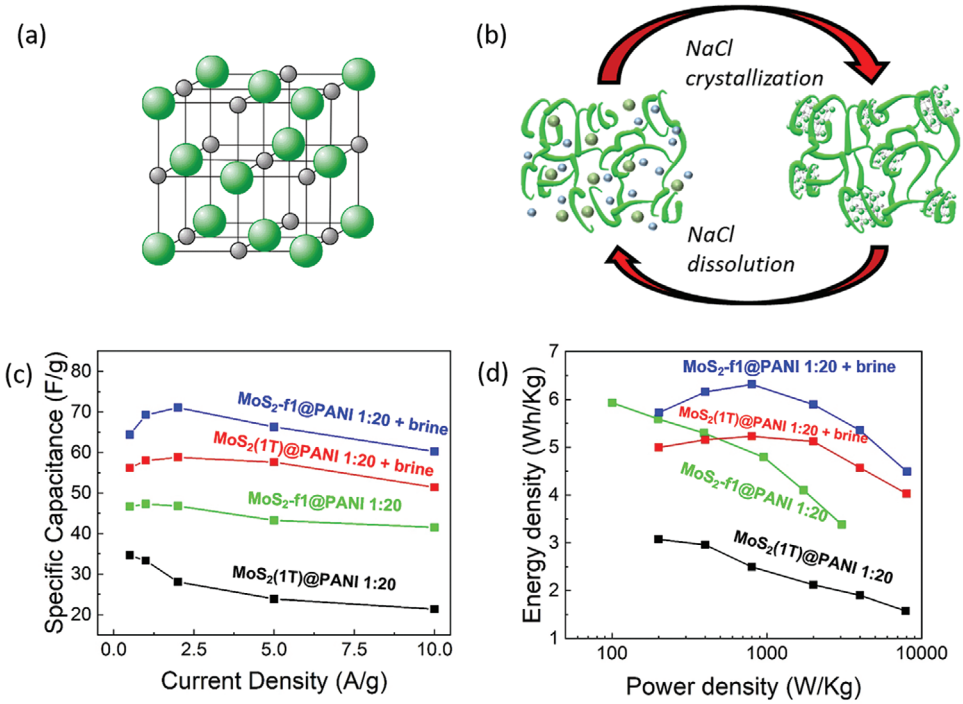

Figure 6. Effect of saturated NaCl (brine) addition during 2D MoS_2/PANI hybrids synthesis on capacitive behavior in a 2-electrodes set-up. a) NaCl crystal structure and b) proposed pseudo-templating mechanism of NaCl during aniline polymerization. c) C_s calculated from GCD curves of the hybrids and d) Ragone plot for the same samples.

Given the promising results in a 3-electrodes setup, further tests were conducted in a 2-electrodes system to more realistically assess the performance of the nanohybrids in an actual supercapacitor-like device. The system chosen for the two-electrode test was assembled in a Swagelok cell, to simulate a device setting with symmetric features and current collectors made of 10 mm diameter Toray paper discs (see Experimental section). In these conditions, both MoS_2-f1@PANI and MoS_2(1T)@PANI species were tested. In addition, two further hybrids were modified by applying NaCl saturated solution (brine) as an additive during the PANI polymerization process, as described in Figure 1, in order to tune functional properties (the two new hybrids are named by simply adding "brine" at the end of MoS_2-f1@PANI and MoS_2(1T)@PANI, for the sake of clarity). The additional salt has no effect on the overall hybrids' morphology (see Figure S9, Supporting Information), but it has been reported to possibly improve the electrochemical performances. NaCl crystals act as pseudo templates (**Figure** 6a,b), as previously reported,[4,46,47] and help establish additional connections between the polymer chains, potentially further enhancing the capacitive behavior of the hybrids. Thus, the brine treatment can be regarded as a soft templating method for nano-structuring of PANI. GCD measurements were performed (Figure S10, Supporting Information) and from them, C_s values were calculated (Figure 6c). The trend observed in the 3-electrodes set-up electrochemical characterization is still visible in the pseudo-device setting. An initial small increase is observed in some samples, likely due to the incomplete stabilization of the composite after the first measurements. This trend might be caused by internal conditioning of the material, which continues even after an initial conditioning process carried out by default on all devices. This process, typically performed around the open circuit potential (OCP), aims to wet the material's surface with the electrolyte. Also, the observed C_s increase during cycling may result from a structural rearrangement occurring at different applied potentials. Specifically, the hybrid based on the covalently functionalized 2D MoS_2 shows a higher C_s compared to the one based on pristine 1T-MoS_2, namely 25% greater at 0.5 A g^{-1} and 45% at 10 A g^{-1} current densities. Moreover, the addition of the NaCl pseudo-template during the synthesis yielded materials with higher C_s (maximum values of 71.1 and 58.8 A g^{-1} for MoS_2-f1@PANI and MoS_2(1T)@PANI, respectively) compared to the one without this pretreatment, proving once again the positive effect of the functionalization of the material, finally obtaining a maximum C_s for the functionalized and brine treated samples of 71.1 F g^{-1} at 0.5 A g^{-1}. This improvement in C_s also results in a larger power and energy density (Figure 6d) for the hybrids prepared in the presence of brine, with 8 kW Kg^{-1} power density and 4.5 Wh Kg^{-1} energy density for the MoS_2-f1@PANI best sample (Table S3, Supporting Information).

To gain insights into the performance retention of the investigated pseudo-capacitors, durability tests were performed on all the above reported samples for over 5000 cycles (**Figure** 7a). Here, the brine-based samples showed a much steeper C_s drop in the early cycles compared to the others, while C_s decreased gradually for the two hybrids prepared without brine until MoS_2-f1@PANI stabilizes at ≈84% retention (best C_s at 5000 cycles among all the functional electrodes tested). It is noticeable that the capacitance of MoS_2(1T)@PANI significantly decreases after ≈2500 cycles. This decline in capacitance is likely due to partial degradation of

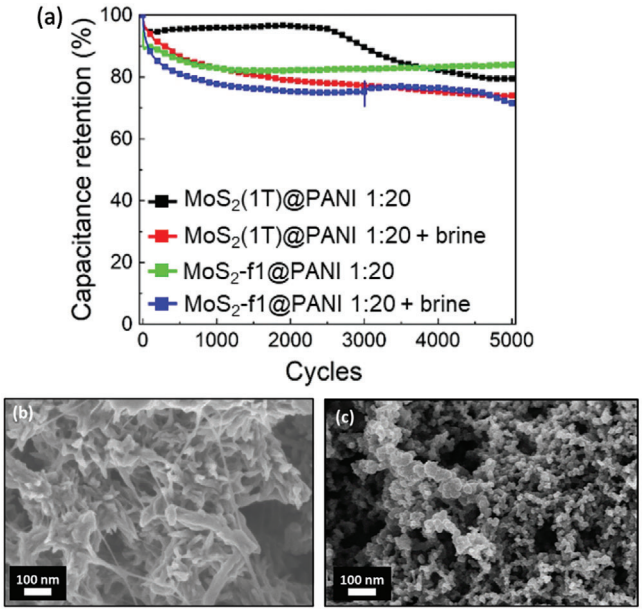

Figure 7. a) Capacitance retention of the different materials in a 2-electrodes set-up. SEM images before b) and after c) cycling for MoS_2-f1@PANI + brine.

PANI or a reduction in the active surface area, which may result from changes in the material's morphology. To further investigate the peculiar deterioration of the brine-based samples, pre- and post-mortem morphological analysis on the electrodes were performed with SEM imaging.

From the SEM image before cycling (Figure 7b), it is possible to observe the presence of thin nanometric polymer-based interconnections within the microstructure of the electrode material. Similar morphological details are not present in the sample prepared without brine, which makes them specific features of the templated samples. However, after cycling these features disappear (Figure 6c), index that they are connected to the charge storage mechanism. We attribute both the increase in C_s and its sharp initial drop during cycling to this morphological variation observed in the nanohybrids prepared with the NaCl pseudo-template. The additional presence of these wires expands the surface where the electrolyte can interact, but, at the same time, the continuous cycling at relatively high current density brings to a rapid degradation of these filaments, leading to a loss in C_s already after 200 cycles. This deterioration in the charge storage performance can be explained in the context of the PANI degradation mechanism, which often encompasses a phase transition corresponding to a morphology change, due to the reversible redox reaction happening in the polymer chains during cycling.[14,48] Therefore, this process may also lead to the disappearance of the nanowires connecting different areas of the composite material, thus reducing the available surface for the energy storage process. This hypothesis is verified by post-mortem SEM images on all samples (Figure 6c; Figure S11, Supporting Information), from which a change in morphology is observed and the degradation of the nanostructure after the cycling occurs. Samples based on pristine 1T-MoS_2 showed the largest morphological difference before and after cycling, with wide areas of the material transitioning to an amorphous microstructure. Simultaneously, the brine pre-treated samples exhibited a lower degree of the amorphous phase, while the filamentous connections disappeared, supporting the aforementioned observations (Figure 7b,c).

Based on the above analysis, the brine treatment appears to positively affect the overall charge storage performance of the hybrid materials, significantly enhancing their C_s. However, this improvement also contributes to a faster capacitance drop in the material. This issue could potentially be addressed by implementing slower cycling conditions or by establishing thicker connections between the polymer chains via longer reaction time, thus reducing the influence of the degradation process, while once again the functionalization proved to yield a better composite in comparison to the non-functionalized samples.

In general, this work produces binary blends starting from a flexible and easy functionalization step of 2D materials. This process was often reported before with graphene[49–51] using diazonium salts, as well as with other 2D materials, such as MXenes[52] and other TMDCs.[45,53,54] This procedure, using iodo-compounds, is not as common but utilizes the same principles, therefore the possibilities for its applications are as wide as the diazonium-based functionalization. In addition, the blending with conductive polymers improves the performance of the single components and their stability. However, blends in literature are often prepared by using three or more components in a non-covalent way (**Table 1**) and therefore, they cannot be compared easily. It is also clear how the 3rd component, usually a carbonaceous material, greatly increases the electrochemical properties. However, our work focuses on the optimization of the interaction between the two basic components, hence introducing a novel promising active material preparation approach with great potential for implementation in stable supercapacitive devices.

3. Conclusion

In summary, this study elucidates two distinct ways for bolstering 2D materials used in electrochemical energy storage. The synthesis of hybrid nanostructures between layered MoS_2 and PANI is reported. This is accomplished by resorting to both pristine 1T-MoS_2 and an easily produced functionalized variant of the MoS_2. The functionalization process occurs under gentle conditions, employing a readily available reagent. It introduces covalently bound aniline moieties, which can be exploited to further tune the structure of the 2D nanosheets by grafting PANI directly on the surface. This functionalization methodology exploits known electrophilic chemistry, which can be also applied to other 2D materials, allowing for material tailoring depending on the final desired application. Notably, the as-synthesized MoS_2-f1@PANI covalent hybrids show better charge storage performance compared to the non-functionalized system in the same way, reaching a specific capacitance of 302.5 F g^{-1} at 0.5 A g^{-1} in a 3-electrodes configuration and demonstrating the power of the grafting approach to improve functionality. Additionally, our investigation also shows that a templating NaCl treatment during synthesis can further improve electrochemical storage capacity, up to 71.5 F g^{-1} at 2 A g^{-1} in a 2-electrodes set-up, compared to 46 F g^{-1} for an analogous sample prepared without such pre-treatment.

Table 1. Literature comparison of the here proposed material with some other binary/ternary blends.

	C_s	Cycle stability (2 electrodes)	Refs.
MoS_2/PANI//CC	452 F g^{-1} (0.2 A g^{-1})	87% (1000 cycles)	[55]
MoS_2/PANI/MnO	469 F g^{-1} (1 A g^{-1})	94.1% (4000 cycles)	[56]
MoS_2/PANI/Graphene	699 F g^{-1} (0.2 A g^{-1})	98.3% (500 cycles)	[57]
MoS_2/PANI	274 A g^{-1} (1 A g^{-1})	42% (1000 cycles)	[41]
MoS_2/PANI/CNT	532 A g^{-1} (1 A g^{-1})	83% (1000 cycles)	
MoS_2/PANI	348 F g^{-1} (0.5 mA cm^{-2})	/	[58]
MoS2/PANI	390 (0.8 A g^{-1})	86% (1000 cycles, 3 Electrodes)	[20]
1T@2H-MoS_2/PANI	618 F g^{-1} (0.5 A g^{-1})	98% (8000 cycles)	[59]
MoS_2-ex/PANI	277 F g^{-1} (0.5 A g^{-1})	98% (10 000 cycles)	[60]
MoS_2-NH_2/PANI	326.4 F g^{-1} (A g^{-1})	96% (10 000 cycles)	[61]
MoS_2-f1/PANI	302.5 F g^{-1} (0.5 A g^{-1})	84% (5000 cycles)	This work

Our results align quite well with those from other 2D material/conducting polymer hybrid systems, providing valuable insights into enhancing 2D materials-based energy storage platforms. We propose an easy-to-make and straightforward method for the covalent functionalization/hybridization of 2D TMDCs. This method can be exploited to produce functional electrodes for reaching high C_s at high current density while maintaining good storage retention over prolonged cycling. Additionally, these hybrids can be easily cast on top of carbon collectors, and, in a similar way, they could be processed on other substrates, even flexible ones, in order to produce a range of energy-storage devices for different electronic applications.

4. Experimental Section

Materials Preparation: MoS_2, Aniline, $(NH_4)_2S_2O_8$, and N-butyl lithium (Li^{n}But) were purchased from Sigma–Aldrich and used without any further purification. p-iodoaniline was purchased from TCI Chemicals and used without any further purification. 1 M HCl was prepared by dilution of concentrated HCl (36–38 wt%) with deionized water and used without any further treatment.

1T MoS_2 Production: 1T-MoS_2 was produced by a slightly modified lithiation procedure reported in the literature.[62,63] A three-neck round bottom flask was connected to an Ar Schlenk line and cleaned following standard Schlenk line procedure (cycles of vacuum, heating, and Ar flux), after which 1 g of bulk MoS_2 and a magnetic stirrer were added under Ar flux in the round bottom flask and left drying under vacuum for 1 h at 40 °C. After drying, the glassware was cooled down using an ice bath, and then 4 mL of dry hexane was added, using an Ar-purged syringe, to the glassware under moderate stirring. Subsequently, 6 mL of Li^{n}But in hexane was added in a similar way to the round bottom flask. The ice bath then, was removed and the solution was left stirring for 3 days at room temperature. At the end of the reaction, the hexane solution was recuperated using hexane as a solvent and centrifuged at 6000 rpm for 20 min, removing the supernatant and adding fresh hexane each time. This procedure was performed three times, and the final tubes were left drying under vacuum at 40 °C overnight. Subsequently, 800 mg of the as lithiated MoS_2 were added to 400 mL of deionized water and exfoliated using a tip-sonicator (TS, Bandelin Sonoplus), operating at 80% power output with 1 s on/1 s off cycles for 2 h while kept at 0 °C with an ice bath. The suspension was then centrifuged at 6000 rpm for 20 min and the supernatant was kept for further work. Furthermore, a set amount was freeze-dried to obtain 1T-MoS_2 powder for further characterization and to calculate the concentration of the suspension, which was 1 mg mL^{-1} on average.

1T-MoS_2 Functionalization: The functionalization was carried out using a previously reported procedure in literature: briefly, a large excess of p-iodoaniline was added to 25 mL of NMF (usually 10 equivalents of the calculated MoS_2 used for the reaction) and left stirring for 15 min at 300 rpm to produce a homogenous pink solution. Afterward, the iodo-aniline solution was added to 100 mL of MoS_2 suspension in a round bottom flask and left stirring for 7 days at 40 °C. After the reaction concluded, the suspension was filtered on a PTFE filter (Omnipore, 200 µm), washed twice with 20 mL of distilled water, once with 10 mL of DMF, and lastly with 10 mL of acetone, and put in a vacuum oven at 40 °C to dry overnight and recuperated the day after.

MoS_2@PANI Hybrids: MoS_2 and PANI hybrids are synthesized according to a common procedure for the PANI polymer. Briefly, two solutions are prepared: in the first one, 10 mg of MoS_2-based material and 12 mg of sodium cholate are added to 6 mL of 1 M HCl and sonicated for 15 min in an ultrasonic bath (USB) at 37 Hz at room temperature. 1T-MoS_2 suspension is prepared for MoS_2(1T)@PANI, and functionalized 1T-MoS_2 suspension is prepared for MoS_2-f1@PANI. Afterward, 114 µL of aniline (1.25 mmol) was added to this suspension and stirred for another 15 min. Simultaneously, another solution was prepared by dissolving 0.3131 g of ammonium peroxydisulfate (APS, 1.1 eq of aniline) in 6 mL of 1 M HCl.

Depending then on the experiment, NaCl was added to both solutions until saturation was reached. The sample as produced has an additional "brine" added to their name and they are respectively: MoS_2(1T)@PANI 1:20 + brine and MoS_2-f1@PANI 1:20 + brine. Once the preparation was over, the aniline/MoS_2 solution was placed in an ice bath to cool it down and the APS solution was then added to it while stirring and left reacting for 1 h. After the reaction, the material was filtered using a paper filter and washed thoroughly with 1 M HCl and, eventually, with 10 mL of acetone and dried in a vacuum oven at 40 °C overnight.

Structural, Chemical, and Morphological Characterization: Raman spectra were recorded on a Bruker Senterra instrument using a 532 nm laser as an excitation source with a power of 0.2 mW, integration time of 5 s, and 60 co-addition per measurement. P-XRD measurements were performed on a PANanalytical B.V. Empyrean in the 5°–75° 2θ range using a step size of 0.013° and an integration time of 100 s. TGA was run on a Netzsch STA409PC instrument, using ≈20 mg per measured sample. Measurements were performed under an inert atmosphere and were heated between 30 °C to 800 °C with a ramp of 10 °C min^{-1}. SEM was performed on a Zeiss Merlin instrument at an acceleration potential of 4 kV, 20 µm beam aperture, and at several different magnifications. The secondary electrons were measured using an in-lens detector and a work distance of 2 mm. HRTEM imaging was conducted with a non-aberration-corrected Transmission Electron Microscope (TALOS F200X, Thermo Scientific, Eindhoven, The Netherlands) operating at 200 kV. The images were acquired using a 16-megapixel CMOS camera with an exposure time of 1 s. EDX was performed with the same

instrument at an acceleration potential varying from 8 to 10 kV, a current of 8 nA, and a 60 µm beam aperture using an X-Max 50 Silicon Drift detector with 50 mm^2 active equipped with a polymer window. XPS measurements were conducted with a PHI 5000 VersaProbe IV Scanning ESCA Microprobe (Physical Electronics) with monochromatized Al Kα 1486.6 eV X-ray source in high power mode (beam diameter 200 µm, X-ray power: 50 W, X-ray lamp voltage: 15 kV). Samples were prepared by filling a Teflon sample cap and attaching them to the XPS sample holder with an isolating tape. A time step of 50 ms, a step size of 0.2 eV, and an analyzer pass energy of 27 eV were used for measuring the detail spectra, while a pass energy of 140 eV was used for the survey spectra. The sample surface was charge neutralized with slow electrons and argon ions, and the pressure was in the range from 10^{-7} to 10^{-6} Pa during the measurement. Data analysis was performed using the CasaXPS software, using an asymmetric Gaussian–Lorentzian function (A(0.35, 0.4, 0) GL(20)) to fit the MoS_2 3d orbitals, while the MoOx 3d and the S 2p orbitals were fitted with a SGL(80) and GL(10) function, respectively.

Electrochemical Characterization: CV was performed in a 3-electrodes set-up using glassy carbon as working, Ag/AgCl as a reference, and a Pt wire as a counter electrode on an Autolab PGSTAT302 equipped with an impedance module. The potential window was chosen by analyzing around the OCP with 100 mV steps until the CE dropped below 95% and confirming the results via CV, resulting in a potential window between 0 and 0.800 V versus Ag/AgCl. PEIS was measured on a fresh electrode at constant potential (OCP), frequency range varying from 1 MHz to 1 Hz, amplitude of 10 mV, and 10 points dec^{-1}. Lastly, PEIS was measured at different potentials (0 and 0.1 V vs Ag/AgCl) after the measure and used for further analysis. GCD measurements were performed between −0.2 and 0.6 V versus Ag/AgCl (ΔV: 0.8 V) at different current densities (0.1–20 A g^{-1}). Specific capacitance was calculated from these measurements using Equation (1):

$$C_s = \frac{I * \Delta t}{m * \Delta V} \quad (1)$$

where I is the discharge current applied, Δt is the discharge time, m is mass in g of active material, and ΔV is the potential window used.

Two electrode measurements were performed using a symmetric setup on a Swagelok cell using a BioLogic SP150 potentiostat. Electrodes were prepared by coating a 10 mm (Swagelok) Toray paper carbon disk with a paste made from the active material, acetylene black and PVDF (mass ratio 8:1:1, respectively), and a glass fiber separator, where tree drops of electrolyte solution (H_2SO_4 0.5 M) were cast. GCD measurements were also performed from 0 to 0.8 V (ΔV: 0.8 V) using current densities (0.1, 0.2, 0.5, 1, 2, 5, and 10 A g^{-1}). Lastly, a stability test was performed on fresh electrodes at 2 A g^{-1} for 5000 cycles, and capacitance retention and faradic efficiency were calculated from the mentioned measurements using the EC Lab program. C_s was calculated by using the aforementioned methodology. Faradic efficiency was calculated by dividing the amount of charge for the discharge and charge part of the GCD curve and reporting them over the course of the cycles.

Lastly, Ragone plot was calculated using Equations (2) and (3) for the energy density (J/g) and the power density (W/g) respectively:

$$E_s = \frac{C_s V^2}{2} \quad (2)$$

$$P_s = \frac{E_s}{t_d} \quad (3)$$

where C_s is the specific capacitance in F/g calculated beforehand, V is the voltage window used for the measurements, E_s is the energy density, and t_d is the discharge time of the GCD curve.

Supporting Information

Supporting Information is available from the Wiley Online Library or from the author.

Acknowledgements

The authors acknowledge the financial support of the European Commission through the H2020 FET-PROACTIVE-EIC-07-2020 project LIGHT-CAP (grant agreement no. [101017821]) and of the European Research Council through the ERC StG project JANUS BI (grant agreement no. [101041229]).

Open access publishing facilitated by Politecnico di Torino, as part of the Wiley - CRUI-CARE agreement.

Conflict of Interest

The authors declare no conflict of interest.

Data Availability Statement

The data that support the findings of this study are available from the corresponding author upon reasonable request.

Keywords

2D MoS_2, capacitive material, covalent functionalization, nanohybrid, polyaniline

Received: July 24, 2024
Revised: September 23, 2024
Published online: October 6, 2024

[1] M. Pershaanaa, S. Bashir, S. Ramesh, K. Ramesh, *J. Energy Storage* **2022**, *50*, 104599.
[2] D. P. Chatterjee, A. K. Nandi, *J. Mater. Chem. A* **2021**, *9*, 15880.
[3] Y. Xu, B. Liu, C. Dong, H. Feng, Y. Wei, X. Zhang, *Eur. J. Inorg. Chem.* **2023**, *26*, e202200569.
[4] M. Crisci, F. Boll, L. Merola, J. J. Pflug, Z. Liu, J. Gallego, F. Lamberti, T. Gatti, *Front. Chem.* **2022**, *10*, 1000910.
[5] R. Zeng, Z. Li, L. Li, Y. Li, J. Huang, Y. Xiao, K. Yuan, Y. Chen, *ACS Sustain. Chem. Eng.* **2019**, *7*, 11540.
[6] Z. Song, Z. Wang, R. Yu, *Small Methods* **2023**, *8*, 2300808.
[7] Z. Song, Z. Wang, R. Yu, *Small Methods* **2024**, *8*, 2300808.
[8] H. Ribeiro, J. P. C. Trigueiro, P. S. Owuor, L. D. Machado, C. F. Woellner, J. J. Pedrotti, Y. M. Jaques, S. Kosolwattana, A. Chipara, W. M. Silva, C. J. R. Silva, D. S. Galvão, N. Chopra, I. N. Odeh, C. S. Tiwary, G. G. Silva, P. M. Ajayan, *Compos. Sci. Technol.* **2018**, *159*, 103.
[9] C. Zhao, X. Jia, K. Shu, C. Yu, G. G. Wallace, C. Wang, *J. Mater. Chem. A* **2020**, *8*, 4677.
[10] S. U. Rahman, P. Röse, A. U. H. A. Shah, U. Krewer, S. Bilal, *Polym.* **2020**, *12*, 2212.
[11] H. Tian, S. Zhu, F. Xu, W. Mao, H. Wei, Y. Mai, X. Feng, *ACS Appl. Mater. Interfaces* **2017**, *9*, 43975.
[12] Q. Zhang, A. Zhou, J. Wang, J. Wu, H. Bai, *Energy Environ. Sci.* **2017**, *10*, 2372.
[13] F. Lai, Z. Fang, L. Cao, W. Li, Z. Lin, P. Zhang, *Ionics* **2020**, *26*, 3015.
[14] H. Tang, Y. Ding, C. Zang, J. Gu, Q. Shen, J. Kan, *Int. J. Electrochem. Sci.* **2014**, *9*, 7239.
[15] O. Öztürk, E. Gür, *ChemElectroChem* **2024**, *11*, 202300575.
[16] S. Manzeli, D. Ovchinnikov, D. Pasquier, O. V. Yazyev, A. Kis, *Nat. Rev. Mater.* **2017**, *2*, 17033.
[17] M. Ali, A. M. Afzal, M. W. Iqbal, S. Mumtaz, M. Imran, F. Ashraf, A. Ur Rehman, F. Muhammad, *Int. J. Energy Res.* **2022**, *46*, 22336.
[18] S. Balendhran, S. Walia, H. Nili, J. Z. Ou, S. Zhuiykov, R. B. Kaner, S. Sriram, M. Bhaskaran, K. Kalantar-Zadeh, *Adv. Funct. Mater.* **2013**, *23*, 3952.

[19] C. Oueiny, S. Berlioz, F. X. Perrin, *Prog. Polym. Sci.* **2014**, *39*, 707.
[20] J. Wang, Z. Wu, K. Hu, X. Chen, H. Yin, *J. Alloys Compd.* **2015**, *619*, 38.
[21] V. Babel, B. L. Hiran, *Polym. Compos.* **2021**, *42*, 3142.
[22] X. Chen, C. Bartlam, V. Lloret, N. M. Badlyan, S. Wolff, R. Gillen, T. Stimpel-Lindner, J. Maultzsch, G. S. Duesberg, K. C. Knirsch, A. Hirsch, *Angew. Chemie Int. Ed.* **2021**, *60*, 13484.
[23] T. Gatti, N. Vicentini, M. Mba, E. Menna, *European J. Org. Chem.* **2016**, *2016*, 1071.
[24] H. Huang, Y. Cui, Q. Li, C. Dun, W. Zhou, W. Huang, L. Chen, C. A. Hewitt, D. L. Carroll, *Nano Energy* **2016**, *26*, 172.
[25] M. Acerce, D. Voiry, M. Chhowalla, *Nat. Nanotechnol.* **2015**, *10*, 313.
[26] Z. Lin, Y. Liu, U. Halim, M. Ding, Y. Liu, Y. Wang, C. Jia, P. Chen, X. Duan, C. Wang, F. Song, M. Li, C. Wan, Y. Huang, X. Duan, *Nature* **2018**, *562*, 254.
[27] H. Li, H. Li, Z. Wu, L. Zhu, C. Li, S. Lin, X. Zhu, Y. Sun, *J. Mater. Sci. Technol.* **2022**, *123*, 34.
[28] D. Tang, J. Li, Z. Yang, X. Jiang, L. Huang, X. Guo, Y. Li, J. Zhu, X. Sun, *Chem. Eng. J.* **2022**, *428*, 130954.
[29] P. Vishnoi, A. Sampath, U. V. Waghmare, C. N. R. Rao, *Chem. – A Eur. J.* **2017**, *23*, 886.
[30] X. Creary, *Chem. Rev.* **1991**, *91*, 1625.
[31] P. W. Ayers, J. S. M. Anderson, J. I. Rodriguez, Z. Jawed, *Phys. Chem. Chem. Phys.* **2005**, *7*, 1918.
[32] R. M. O'Ferrall, *Adv. Phys. Org. Chem.* **2010**, *44*, 19.
[33] O. of D. I. (ODI), U. . D. of C., National Institute of Science and Technology (NIST), https://srdata.nist.gov/xps/SpectraIdentifier.
[34] R. A. Meyers, in *Encyclopedia of Analytical Chemistry*, Wiley, USA **2007**.
[35] C. Tsioptsias, *Measurement* **2022**, *204*, 112136.
[36] D. Lee, K. Char, *Polym. Degrad. Stab.* **2002**, *75*, 555.
[37] A. Kumar, A. Kumar, H. Mudila, K. Awasthi, V. Kumar, *J. Phys. Conf. Ser.* **2020**, *1531*, 012108.
[38] A.ul. H. Ali Shah, N. Yasmeen, G. Rahman, S. Bilal, *Electrochim. Acta* **2017**, *224*, 468.
[39] A. H. A. Shah, S. Akhlaq, M. Sayed, S. Bilal, N. Ali, *Chem. Pap.* **2018**, *72*, 2523.
[40] K. Pandey, P. Yadav, I. Mukhopadhyay, *Phys. Chem. Chem. Phys.* **2014**, *17*, 878.
[41] M. Jasna, M. Muraleedharan Pillai, A. Abhilash, P. S. Midhun, S. Jayalekshmi, M. K. Jayaraj, *Carbon Trends* **2022**, *7*, 100154.
[42] V. Vivier, M. E. Orazem, *Chem. Rev.* **2022**, *122*, 11131.
[43] J. Huang, *Electrochim. Acta* **2018**, *281*, 170.
[44] Q. Tang, D. E. Jiang, *Chem. Mater.* **2015**, *27*, 3743.
[45] H. Zhang, T. D. Koledin, W. Xiang, J. Hao, S. U. Nanayakkara, N. H. Attanayake, Z. Li, M. V. Mirkin, E. M. Miller, *2D Mater.* **2021**, *9*, 015033.
[46] A. Chellachamy Anbalagan, S. N. Sawant, *Polymer* **2016**, *87*, 129.
[47] A. Singh, M. Moun, M. Sharma, A. Barman, A. Kumar Kapoor, R. Singh, *Appl. Surf. Sci.* **2021**, *538*, 148201.
[48] A. Q. Zhang, C. Q. Cui, J. Y. Lee, *Synth. Met.* **1995**, *72*, 217.
[49] G. L. C. Paulus, Q. H. Wang, M. S. Strano, *Acc. Chem. Res.* **2012**, *46*, 160.
[50] A. Sinitskii, A. Dimiev, D. A. Corley, A. A. Fursina, D. V. Kosynkin, J. M. Tour, *ACS Nano* **2010**, *4*, 1949.
[51] G. L. C. Paulus, Q. H. Wang, M. S. Strano, *Acc. Chem. Res.* **2013**, *46*, 160.
[52] D. Sabaghi, J. Polčák, H. Yang, X. Li, A. Morag, D. Li, A. S. Nia, S. Khosravi H, T. Šikola, X. Feng, M. Yu, *Adv. Energy Mater.* **2024**, *14*, 02961.
[53] L. Daukiya, J. Teyssandier, S. Eyley, S. El Kazzi, M. C. Rodríguez González, B. Pradhan, W. Thielemans, J. Hofkens, S. De Feyter, *Nanoscale* **2021**, *13*, 2972.
[54] A. A. Mohamed, Z. Salmi, S. A. Dahoumane, A. Mekki, B. Carbonnier, M. M. Chehimi, *Adv. Colloid Interface Sci.* **2015**, *225*, 16.
[55] Y. Wang, X. Lv, S. Zou, X. Lin, Y. Ni, *RSC Adv.* **2021**, *11*, 10941.
[56] H. Heydari, M. Abdouss, S. Mazinani, A. M. Bazargan, F. Fatemi, *J. Energy Storage* **2021**, *40*, 102738.
[57] S. Palsaniya, H. B. Nemade, A. K. Dasmahapatra, *Polymer* **2018**, *150*, 150.
[58] S. Krithika, J. Balavijayalakshmi, *Mater. Today Proc* **2022**, *50*, 17.
[59] R. Rahman, P. Rani, S. Ghosh, A. Midya, A. Pathak, T. K. Nath, *ACS Appl. Energy Mater.* **2023**, *6*, 11012.
[60] M. Tomy, M. A. Anu, T. S. Xavier, *Appl. Phys. A Mater. Sci. Process.* **2023**, *129*, 1.
[61] R. Zeng, Z. Li, L. Li, Y. Li, J. Huang, Y. Xiao, K. Yuan, Y. Chen, *ACS Sustain. Chem. Eng.* **2019**, *7*, 11540.
[62] A. Ambrosi, Z. Sofer, M. Pumera, *Small* **2015**, *11*, 605.
[63] S. Jayabal, J. Wu, J. Chen, D. Geng, X. Meng, *Mater. Today Energy* **2018**, *10*, 264.